5-1-2003

CO Emission from Disks around AB Aurigae and HD 141569: Implications for Disk Structure and Planet Formation Timescales

Sean D. Brittain
Clemson University, sbritt@clemson.edu

Terrence W. Rettig
University of Notre Dame

Theodore Simon
University of Hawaii

Craig Kulesa
University of Arizona

Michael A. DiSanti
NASA Goddard Space Flight Center

See next page for additional authors

The Astrophysical Journal, 588:535–544, 2003 May 1

CO EMISSION FROM DISKS AROUND AB AURIGAE AND HD 141569: IMPLICATIONS FOR DISK STRUCTURE AND PLANET FORMATION TIMESCALES

Sean D. Brittain and Terrence W. Rettig[1,2]
Center for Astrophysics, University of Notre Dame, Notre Dame, IN 46556; trettig@nd.edu, sbrittai@nd.edu

Theodore Simon[2]
Institute for Astronomy, University of Hawaii, 2680 Woodlawn Drive, Honolulu, HI 96822

Craig Kulesa
University of Arizona, Steward Observatory, 933 North Cherry Avenue, Tucson, AZ 85721

Michael A. DiSanti
NASA Goddard Space Flight Center, Laboratory for Extraterrestrial Physics, Greenbelt, MD 20771

and

Neil Dello Russo
Department of Physics, Catholic University of America, Washington, DC; and NASA Goddard Space Flight Center, Laboratory for Extraterrestrial Physics, Greenbelt, MD 20771
Received 2002 January 28; accepted 2003 January 7

ABSTRACT

We present a comparison of CO fundamental rovibrational lines (observed in the *M* band near 4.7 μm) from the inner circumstellar disks around the Herbig AeBe stars AB Aur and HD 141569. The CO spatial profiles and temperatures constrain the location of the gas for both stars to a distance of less than 50 AU. The CO emission from the disk of the $\sim$4 Myr star AB Aur shows at least two temperature components, the inner disk at a rotational temperature of 1540 ± 80 K and the outer disk at 70 ± 10 K. The hot gas is located near the hot bright inner rim of the disk and the cold gas is located in the outer disk from 8–50 AU. The relative intensities of low-*J* lines suggest that the cold gas is optically thick. The excitation of CO in both temperature regimes is dominated by infrared fluorescence (resonant scattering). In the more evolved disk around HD 141569, the CO is excited by UV fluorescence. The relative intensity of the CO emission lines implies a rotational temperature of 190 ± 30 K. The resulting column density is $\sim 10^{11}$ cm^{-2}, indicating approximately 10^{19} g of CO. The observed line profiles indicate that the inner disk has been cleared of CO gas by stellar radiation out to a minimum of 17 AU. The residual mass of CO suggests that the inner disk of HD 141569 is not in an active phase of planet building but it does not rule out the possibility that giant planet building has previously occurred.

Subject headings: circumstellar matter — ISM: molecules — planetary systems: protoplanetary disks

1. INTRODUCTION

Planet formation has been known for many years to be tied to the accretion and evolution of gas and dust in disks around young stars. Herbig AeBe (HAeBe) stars represent an ideal laboratory for studies of disk evolution and planet formation. They are 2–10 $M_\odot$ pre–main-sequence stars (Waters & Waelkens 1998) with large extended disks (Hillenbrand et al. 1992; Mannings & Sargent 1997; Weinberger et al. 2000; Natta et al. 2000). These young objects have spectral types of F0 or earlier, broad infrared excesses due to circumstellar dust, and atomic emission lines (e.g., Herbig 1960; Finkenzeller & Mundt 1984; Waters & Waelkens 1998; van den Ancker 1999). The physical parameters of HAeBe disks constrain the duration of the protoplanetary phase and the age at which the signatures of planets become visible in circumstellar disks (Grady et al. 1999). HAeBe stars have been studied extensively at various wavelengths, from the X-ray to the radio. However, little spectroscopic work has been done in the near-infrared, particularly in the *M* band near 5 μm. The high thermal background and variable transparency of the earth's atmosphere make observations at this wavelength especially challenging (see Najita et al. 2000).

This paper presents high-resolution near-infrared spectral observations of the $v = 1$–0 rovibrational band of CO near 4.7 μm for the HAeBe stars AB Aur (HD 31293) and HD 141569. Of particular interest to this work is the gas content and temperature structure of the disk region of these stars ($<$50 AU) where Jovian-type planets may form. For a pre–main-sequence star with an age of 2–4 Myr, similar to AB Aur, the strong infrared excess in the spectral energy distribution (SED) suggests that the disk has not been significantly dissipated by radiation pressure, Poynting-Robertson drag, collisions, or sublimation (Backman & Paresce 1993). This young disk may not yet have progressed to the gas-accretion phase of planet building, but the material in the inner region is likely being sculpted by accretion processes. At an age similar to that of HD 141569 ($\sim$5 Myr or older), the disk begins to resemble a more mature

[1] Visiting Astronomer at the Infrared Telescope Facility, which is operated by the University of Hawaii under contract from the National Aeronautics and Space Administration.

[2] Visiting Astronomer at the W. M. Keck Observatory, which is operated as a scientific partnership among the California Institute of Technology, the University of California, and the National Aeronautics and Space Administration. The Observatory was made possible by the generous financial support of the W. M. Keck Foundation.

planetary system, having mostly cleared the inner region of dust and gas, as exhibited by the minimal IR excess. The CO content and location has important implications for models of the disk evolution and planet formation timescales (Najita et al. 1996, 2000; Carr et al. 2001)

1.1. *AB Aur*

AB Aur (HD 31293) is one of the nearest, brightest, and best studied of the Herbig HAeBe class of pre–main-sequence stars. It has a distance of 144 pc (van den Ancker, de Winter, & Tjin A Djie 1998), a spectral type of A0 Ve+sh (Thé et al. 1994), and a disk that extends to a radius of more than 10^3 AU (Nakajima & Golimowski 1995; Grady et al. 1999). The outer regions of the disk have been imaged at a variety of wavelengths, including millimeter (Mannings & Sargent 1997), mid-IR (Marsh et al. 1995), and near-IR (Millan-Gabet et al. 1999, 2001). The inclination of the disk of AB Aur is somewhat uncertain. The millimeter interferometric data taken by Mannings & Sargent suggest that the inclination of the disk with respect to the plane of the sky is 76°; however, Grady et al. (1999) demonstrate that the inclination of the disk is likely less than 45°. A nearly pole-on orientation of the disk is consistent with near-infrared (NIR) observations of the inner disk ($r < 0.5$ AU) by Millan-Gabet et al. (1999). Modeling by Natta et al. (2001) indicates an inclination of 30°, which we demonstrate may be an upper limit. The age of AB Aur, from its location on the HR diagram, is constrained to 2–4 Myr by van den Ancker et al. (1998) and to 4.6 Myr by Thi et al. (2001). In this rather young HAeBe star, dusty material in the disk dominates the infrared flux, leading to an excess in the observed SED (Malfait et al. 1998). The components of the dust are amorphous silicates, iron oxide, and PAHs (van den Ancker et al. 1998; Bouwman et al. 2000). The dust- and gas-rich circumstellar disk is highly opaque to UV radiation from the protostar, which may limit the effect of UV radiation on chemical processing of the disk material at large distances (Prinn 1993).

A number of models have been proposed over the last two decades to describe the infrared excesses associated with pre–main-sequence stars (e.g., Chiang & Goldreich 1999; Chiang et al. 2001; Natta et al. 2001 and references therein). In most cases, the mid- and far-infrared region of the SEDs can be described by the flared-disk model, but it is unable to account for the 2 μm "bump" (Natta et al. 2001). In a variation of the flared-disk model, Dullemond et al. (2001) showed that the inner edge of the truncated disk, which is directly exposed to stellar radiation, is a "puffed-up" region with a larger vertical scale height. For AB Aur, the resulting higher rim temperature, at a distance of 0.5 AU, provides an adequate explanation for the 2 μm feature. The model also predicts that the outer flared disk emerges from the rim shadow at 8 AU. In this work, we report results from infrared CO emission lines that originate from two distinct regions in the inner disk.

1.2. *HD 141569*

The HAeBe star HD 141569 is an isolated, nearby (99 pc), 5–8 Myr old B9.5 Ve/A0 star/disk system that is best understood as a transitional object passing from the pre–main sequence to the zero-age main sequence (van den Ancker et al. 1998; Weinberger et al. 2000; Fisher et al. 2000). With an infrared excess as well as emission from Hα and [O I], it satisfies most of the HAeBe criteria. The Paschen series, however, is seen in absorption, and the ratio of the infrared to stellar luminosity, 8×10^{-3}, is similar to the main-sequence object β Pic (Dunkin et al. 1997; Fisher et al. 2000). The small excess in the infrared SED suggests that much of the dust in the inner region has been dissipated. The disk is inclined by $39° \pm 3°$ (with respect to the plane of the sky) and has a 400 AU radius with a large gap at 250 AU; radio observations indicate that the CO gas is confined to the region inside this gap (Weinberger et al. 1999; Zuckerman et al. 1995). *Hubble Space Telescope* STIS coronagraphic observations reveal a highly asymmetric system with two ringlike structures at 200 and 325 AU; the region from 125 to 175 AU is devoid of material (Mouillet et al. 2001).

The inner planet-forming region of HD 141569 is mostly cleared of gas and dust but still may contain a record of processed material that is released as a result of collisions and heating of residual planetesimals and grains (Backman & Paresce 1993; Zuckerman & Becklin 1993; Sylvester et al. 1996). While the SED implies that the inner 10 AU is cleared (Malfait et al. 1998), thermal mid-IR imaging at 10.8 and 18.2 μm provides evidence for the presence of dust grains (smaller than 2 μm) out to radial distances of $\sim$100 AU (Fischer et al. 2000). Dust of this size has a short disk lifetime; therefore, the mid-IR–emitting grains are not primordial and must have been replenished through collisions of larger particles on a timescale of 10^2–10^4 yr (Weinberger et al. 2000; Fischer et al. 2000). The existence of gas and small dust grains, in the presence of forces that remove them quickly, is indicative of a disk in an active planet/planetesimal building phase (Weinberger et al. 1999). Because the morphological data is of insufficient resolution, the structure and evolution of the disk remains speculative. The CO emission lines analyzed in § 4 originate from a region in the disk beyond 17 AU.

2. OBSERVATIONS

Emission spectra of CO are presented in Figure 1 for AB Aur and in Figure 2 for HD 141569. The observations for AB Aur were obtained at both the NASA Infrared Telescope Facility (IRTF) and the W. M. Keck Observatory. All of the CO spectra presented for HD 141569 were obtained at the IRTF. The cryogenic echelle spectrograph (CSHELL: Tokunaga et al. 1990) at the IRTF provided a resolving power (RP) of 21,500. The NIRSPEC echelle spectrograph (McLean et al. 1998) at Keck 2 provided RP = 25,000. The observations at both facilities are summarized in Table 1. A series of flats and darks were used to remove systematic effects at each grating setting. The two-dimensional frames were cleaned of systematically hot and dead pixels as well as cosmic-ray hits, and were then resampled spatially and spectrally. This initial processing results in frames for which spectral and spatial dimensions are orthogonal, falling along rows and columns, respectively (DiSanti et al. 2001). Absolute flux calibration was achieved through observations of standard stars. All of the spectral extracts presented in these figures are constrained to the inner 50 AU of the disk for both AB Aur and HD 141569.

The *M*-band spectra are dominated by a significant thermal ($\sim$300 K) continuum background, upon which are superimposed night-sky emission lines. The intensities of

TABLE 1
JOURNAL OF OBSERVATIONS

Telescope/Instrument	Date	Setting/Order	Spectral range (cm^{-1})	Integration (minutes)	S/N
		HD 141569			
IRTF (CSHELL).....	2001 Aug 6		2097–2103	48	13
			2122–2128	60	15
	2001 Aug 7		2108–2113	48	9
			2145–2151	40	10
	2001 Aug 9		2160–2166	20	4
		AB Aur			
IRTF (CSHELL).....	2001 Aug 9		2120–2126	20	18
			2146–2152	20	30
Keck II (NIRSPEC).....	2002 Mar 21	16	2125–2158	4	300
		15	1992–2024	4	100
	2002 Mar 21	16	2095–2127	16	150
		15	1965–1995	16	100
	2002 Nov 16	16	2035–2062	20	110

these telluric lines depend not only on the air mass, but also on the column burden of atmospheric water vapor, which can vary both temporally and spatially over the course of the night. In order to cancel most of the atmospheric+background, the telescope was nodded by a small distance, typically 15″, along the slit. The nod pattern was typically from the north position (A) to the south position (B) in an {A, B, B, A} sequence, with each step corresponding to 1 minute of

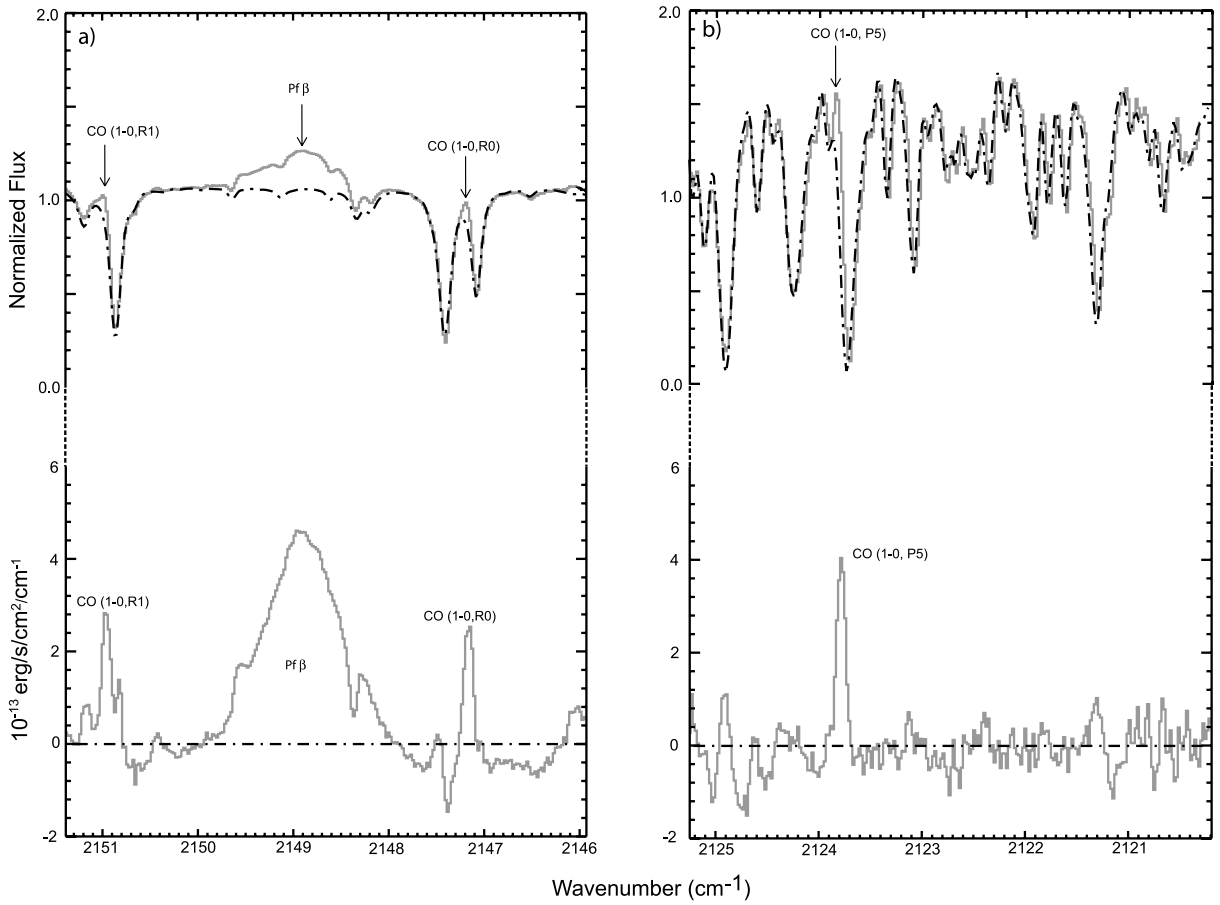

FIG. 1.—CO spectral extracts of AB Aur obtained (*a*, *b*) with CSHELL at the IRTF and (*c*–*g*) with NIRSPEC at KECK II . The spectral resolving power (RP = 2.5×10^4) was sufficient to detect multiple CO (1–0) rovibrational emissions. The broad hydrogen line (Pfβ) in (*a*) with velocity broadening of ~130 km s^{-1} (FWHM of 0.96 cm^{-1}) suggests an active stellar wind. The flux of Pfβ line in AB Aur increased by about 80% from 2001 to 2002, while the CO emission features remained constant. The residuals for (*a*) and (*b*) are presented below the spectral extracts. The telluric model is indicated by a black dash–dotted line, and the data are shown by a gray solid line.

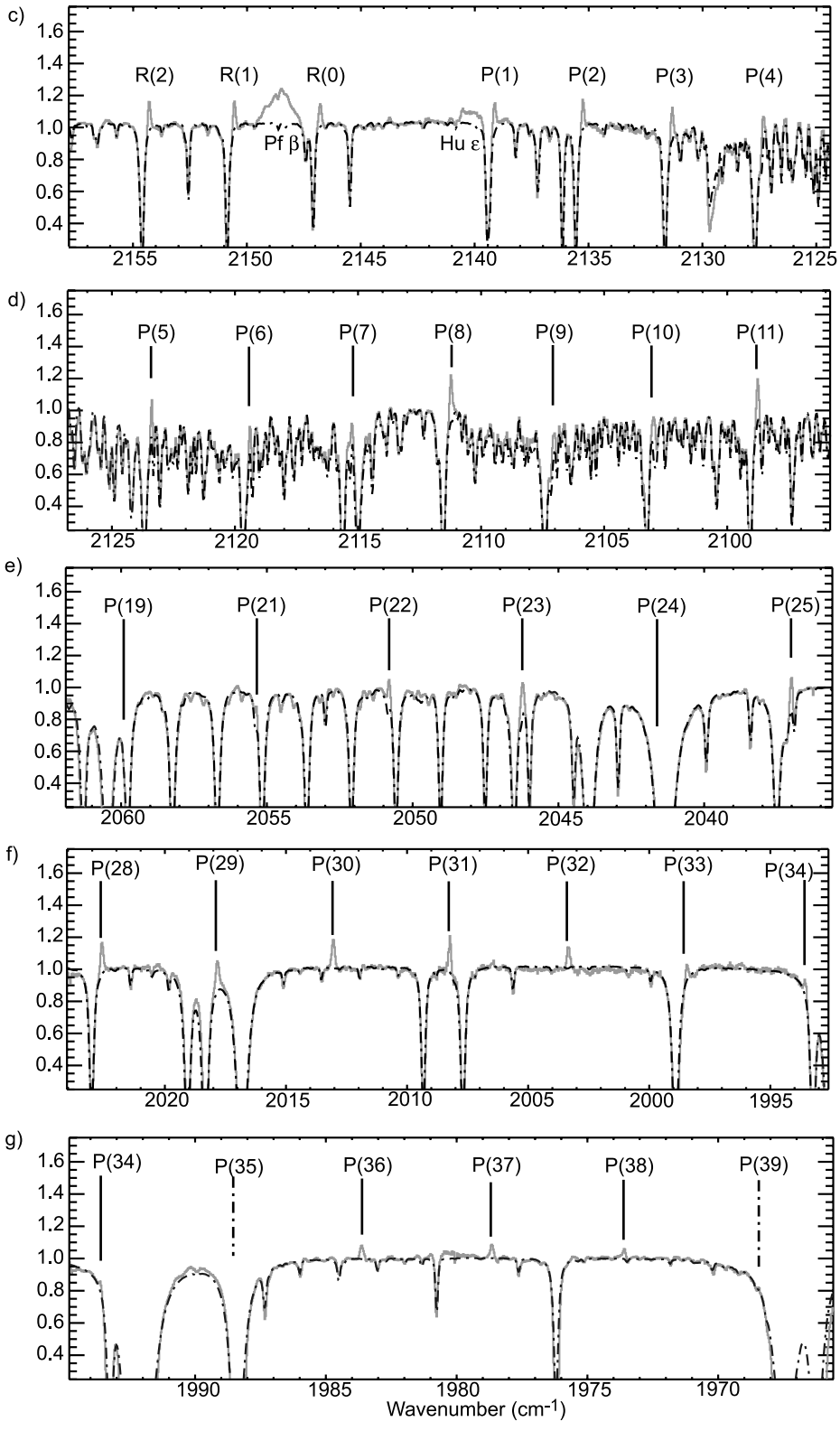

FIG. 1.—*Continued*

integration time. Combining the scans as {A−B−B+A}/2 cancels the telluric features to first order. Subsequently, the FWHM of the spatial profiles in the A and B rows are extracted to obtain the spectra for both positions. The atmospheric transmittance function of the combined spectrum was modeled using the Spectrum Synthesis Program (SSP; Kunde & Maguire 1974), which accesses the '92HITRAN molecular database (Rothman 1992). For each grating setting listed in Table 1, the optimized model establishes the column burden of absorbing atmospheric species, the spectral resolving power, and the wavelength calibration. Subtraction of the optimized model (scaled to

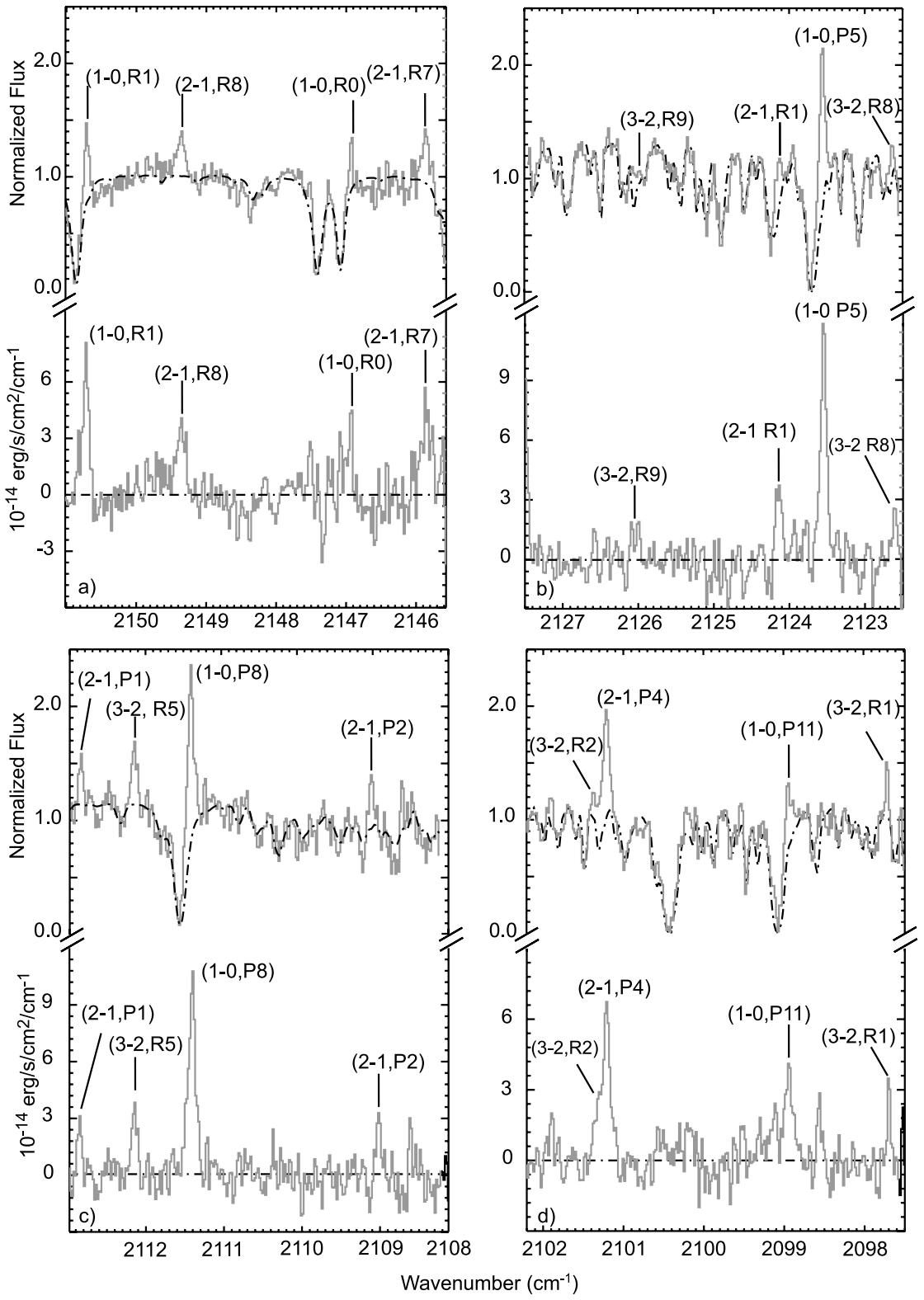

FIG. 2.—CO spectral extracts of HD 141569 acquired with CSHELL at the IRTF at a RP = 21,500. The residuals are presented below each spectrum. The $v = 1$–0, 2–1, and 3–2 lines are labeled. The telluric model is indicated by a black dotted line, and the data are shown by a gray solid line.

the observed continuum) reveals the residual spectrum of emission lines. Examples of modeled spectral extracts, as well as residuals, are shown in Figures 1 and 2.

Each line is divided by the atmospheric transmittance at the Doppler-shifted line center frequency to calculate the intensity of the emission lines above the atmosphere. Table 2 presents observed position, rest position, transmittance, and flux for CO lines in AB Aur and HD 141569. For many emission lines, the uncertainty in transmittance dominates the uncertainty in the corrected line flux. The transmittance

TABLE 2
Observed and Rest Position, Transmittance, and Measured Flux for Each CO Line

Line ID	$\tilde{\nu}_{obs}$ (cm^{-1})	$\tilde{\nu}_{rest}$ (cm^{-1})	$\%T$	$F \pm \delta F$[a] ($W\ m^{-2}$)
		AB Aur		
$R(2)$.....	2154.27	2154.60	0.93	(1.0 ± 0.1)E−16
$R(1)$[b]	2150.96	2150.86	0.66	(1.0 ± 0.1)E−16
$R(1)$.....	2150.54	2150.86	0.95	(8.6 ± 1.0)E−17
$R(0)$.....	2146.78	2147.08	0.97	(8.8 ± 1.0)E−17
$R(0)$[b]	2147.17	2147.08	0.71	(7.7 ± 0.5)E−17
$P(1)$.....	2139.11	2139.43	0.92	(1.5 ± 0.1)E−16
$P(2)$.....	2135.22	2135.55	0.95	(9.9 ± 1.0)E−17
$P(3)$.....	2131.33	2131.63	0.74	(1.4 ± 0.1)E−16
$P(4)$.....	2127.38	2127.68	0.45	(2.1 ± 1.0)E−16
$P(5)$.....	2123.37	2123.70	0.89	(1.2 ± 0.1)E−16
$P(5)$[b]	2123.80	2123.70	0.50	(1.22 ± 0.07)E−16
$P(6)$.....	2119.34	2119.68	0.76	(1.38 ± 0.14)E−16
$P(7)$.....	2115.31	2115.63	0.50	(1.75 ± 0.22)E−16
$P(8)$.....	2111.23	2111.54	0.92	(1.6 ± 0.1)E−16
$P(9)$.....	2107.11	2107.42	0.57	(1.4 ± 0.2)E−16
$P(10)$.....	2102.96	2103.27	0.78	(1.78 ± 0.14)E−16
$P(11)$.....	2098.76	2099.08	0.91	(1.35 ± 0.12)E−16
$P(20)$[c].....	2059.87	2059.91	0.30	(1.4 ± 0.5)E−16
$P(21)$[c].....	2055.35	2055.40	0.75	(8.3 ± 2.4)E−17
$P(22)$[c].....	2050.81	2050.85	0.82	(1.0 ± 0.2)E−16
$P(23)$[c].....	2046.25	2046.28	0.78	(1.2 ± 0.2)E−16
$P(24)$[c].....	2041.65	2041.67	0.10	(2.7 ± 1.7)E−16
$P(25)$[c].....	2036.99	2037.03	0.86	(9.0 ± 0.8)E−17
$P(28)$.....	2022.63	2022.91	0.93	(9.6 ± 0.9)E−17
$P(29)$.....	2017.86	2018.15	0.78	(9.8 ± 1.0)E−17
$P(30)$.....	2013.05	2013.35	0.98	(8.9 ± 0.8)E−18
$P(31)$.....	2008.25	2008.53	0.94	(7.1 ± 0.9)E−17
$P(32)$.....	2003.34	2003.67	0.97	(6.5 ± 0.8)E−17
$P(33)$.....	1998.47	1998.78	0.86	(6.3 ± 0.9)E−17
$P(34)$.....	1993.56	1993.86	0.74	(6.1 ± 1.1)E−17
$P(36)$.....	1983.63	1983.94	0.99	(4.9 ± 0.9)E−17
$P(37)$.....	1978.67	1978.93	0.99	(4.4 ± 0.9)E−17
$P(38)$.....	1973.60	1973.89	0.99	(2.8 ± 0.9)E−17
		HD 141569		
$R(5)$.....	2165.45	2165.60	0.49	(1.1±0.2)E−17
$R(1)$.....	2150.72	2150.86	0.72	(5.9±0.8)E−18
$R(0)$.....	2146.93	2147.08	0.84	(3.3±0.7)E−18
$P(5)$.....	2123.57	2123.70	0.56	(1.4±0.1)E−17
$P(8)$.....	2111.41	2111.54	0.70	(1.1±0.1)E−17
$P(11)$.....	2098.96	2099.08	0.62	(7.2±0.8)E−18

[a] The fluxes include a transmittance correction.
[b] Lines observed with CSHELL on IRTF.
[c] Data taken 2002 Nov 16 with NIRSPEC on Keck II.

can vary greatly over a small frequency interval because of the number of telluric features near the emission line. The uncertainty in Doppler-shifted line position is determined from the standard deviation of the Doppler shifts for each of the emission lines. Once the line position is measured, the uncertainties in transmittance and flux are determined from the fully resolved SSP model. The stochastic (photon) noise is added in quadrature to the transmittance uncertainty.

3. CO IN AB AUR

Spectral extracts of CO in AB Aur are presented in Figure 1. Figures 1*a* and 1*b* present the CO observations from the IRTF in 2001 August. Figures 1*c*–1*g* present the observations acquired at KECK II in 2002 March and November. The broad H I Pfβ emission line at 2149 cm^{-1} in Figures 1*a* and 1*c* indicates a stellar wind associated with the central star. The line is structurally similar to other atomic transitions seen by Catala et al. (1986). Typically, these are broad emission features with superimposed absorption lines that tend to be highly variable. The flux of the Pfβ line in AB Aur increased by about 80% from 2001 to 2002, while the CO emission features remained constant.

An analysis of observed frequencies for the CO emission lines from AB Aur with respect to the telluric CO line positions in Figures 1*a* and 1*b* provides a heliocentric radial velocity of the system of $+12 \pm 3$ km s^{-1} (i.e., after correction for the motion of the earth). From Figures 1*c*–1*g*, the resulting heliocentric velocity of the CO is $+11 \pm 2$ km s^{-1}. Both are consistent with CO velocity measurements from STIS ($+10 \pm 3$ km s^{-1}; Roberge et al. 2001) and indicate the gas we are detecting is associated with the star. The Doppler shift and width of all the lines are consistent with one another and the STIS data.

An A0 star has sufficient UV flux radiating the inner disk to excite CO bands of the fourth positive system ($A^1\Pi$–$X^1\Sigma^+$). When this band relaxes to the ground electronic state, the vibrational levels $v' = 1$, 2, and 3 are expected to be nearly evenly populated (Mumma, Stone, & Zipf 1971). Indeed, the CO spectrum from HD 141569 demonstrates UV excitation (§ 4). However, in the observations of AB Aur, only the $v = 1$–0 transitions of CO are detected (Fig. 1). The observed upper limit for the $v = 2$–1 transitions is less than 10% of the intensity of the $v = 1$–0 transitions. In this case, the UV must be quenched before it can reach significant quantities of CO in the disk. Following calculations by Gonzalez-Alfonso et al. (2002), the excitation rate due to infrared fluorescence (resonant scattering) exceeds that due to collisions.

The infrared fluorescence that dominates the excitation of CO around AB Aur is similar to that seen in solar system comets. For comets at 1 AU, the fluorescence efficiency to the $v' = 1$ level (g_{0-1}) is 2 orders of magnitude greater than to the $v' = 2$ level (g_{0-2}) (Crovisier & Le Bourlot 1983). Given the comparatively low UV flux of the Sun, the UV fluorescent efficiency (g_{X-A}) is also about 2 orders of magnitude lower than g_{0-1} (Feldman et al. 1976), so the population of $v' = 2$ by relaxation of electronically excited CO does not significantly contribute to the rovibrational spectrum.

Approximating CO as a rigid rotor, one can demonstrate that the flux of an emission line is

$$F_J = \Omega I_{em} = \frac{\Omega C_{em}}{Q_r} \tilde{\nu}^4 (J' + J'' + 1) e^{-BJ'(J'+1)hc/kT} ,$$

and thus

$$\frac{k}{hcB} \ln\left[\frac{F_J}{\tilde{\nu}^4 (J' + J'' + 1)}\right] = -\frac{1}{T} J'(J' + 1) + \frac{k}{hcB} \ln \frac{\Omega C_{em}}{Q_r} .$$

Here k is the Boltzmann constant, h is the Planck constant, c is the speed of light, B is a rotational constant, F_J is the measured flux of each line, J' is the upper transition state, J'' the lower state, T is the temperature of the gas, C_{em} is a spectroscopic constant, Ω is the solid angle subtended by the beam, and Q_r is the partition function for a rigid rotor (Herzberg 1950). Figure 3 plots $J'(J' + 1)$ versus $(k/hcB)\ln[F_J/\tilde{\nu}^4 (J' + J'' + 1)]$ for AB Aur and HD 141569; the rotational

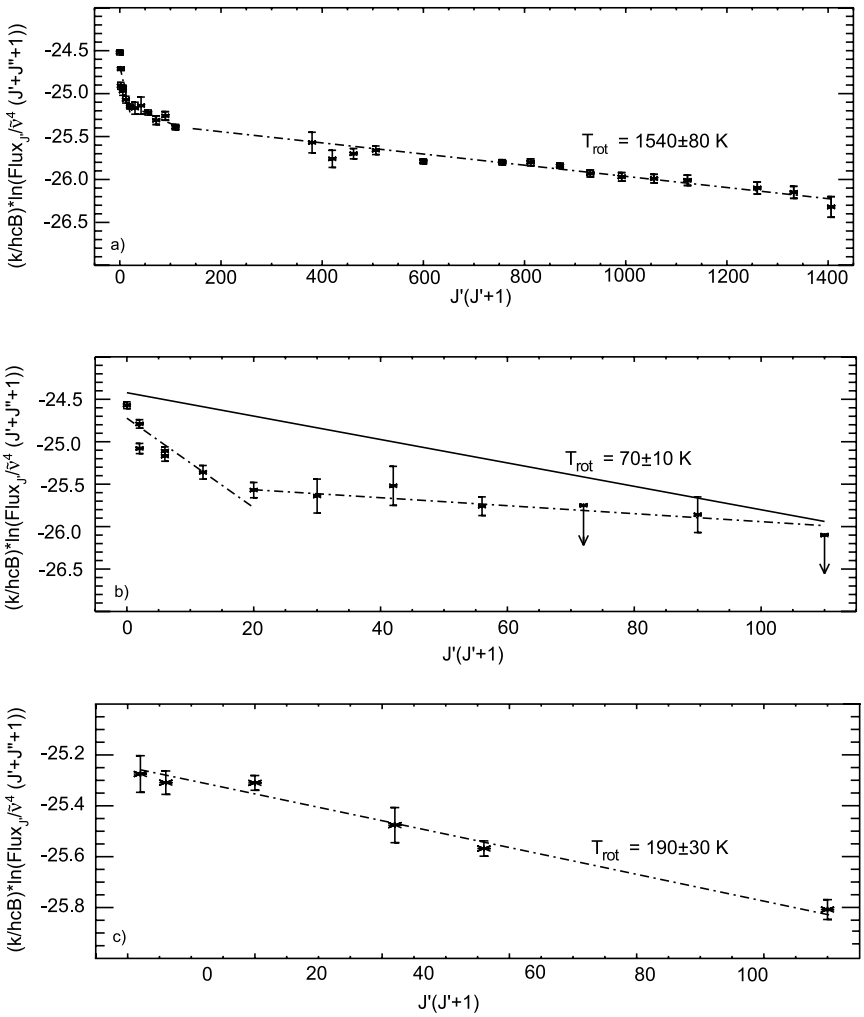

FIG. 3.—Rotational temperatures of CO for AB Aur and HD 141569. Panel *a* presents the CO lines for AB Aur spanning $J' = 0$–37. The low-J lines ($J' = 0$–10) show a considerably steeper slope (lower temperature) than the high-J lines ($J' = 19$–37), indicating both cold- and hot-gas components are present in our beam. The rotational temperature of the hot gas (determined from a linear fit to the $J' = 19$–37 lines) is 1540 ± 80 K. Panel *b* shows an expanded view of the low-J ($J' = 0$–10) lines for AB Aur after subtracting the intensity contributed by the hot gas. The extrapolation suggests that the flux of the $P(9)$–$P(11)$ lines is largely due to the hot gas and is presented as upper limits. In this case, the discontinuity near the $P(5)$ line [$J' = 4$ or $J'(J' + 1) = 20$] results from optically thick gas. The corrected fit, illustrated as a solid line, provides a rotational temperature of 70 K for the cold gas. Panel *c* presents the CO lines for HD 141569 spanning $J = 1$–10 and a resulting rotational temperature of 190 K.

temperature is defined by the negative reciprocal of the linear least-squares slope.

Figure 3*a* presents CO data for AB Aur spanning $J' = 0$–37. The data can be fitted by three slopes from $J' = 0$–5, 5–10, and 19–37. These discontinuities can be described by optically thick lines and/or a temperature gradient in the source (e.g., Mitchell et al. 1990; van der Tak et al. 2000). The levels $J' > 19$ are not sufficiently populated to contribute to line opacity and cannot explain the break at high J. Therefore, both cold- and hot-gas components are present in our beam. The rotational temperature of the hot gas (determined from a linear fit to the $J' = 19$–37 lines) is 1540 ± 80 K.

To determine the rotational temperature of the gas described by the low-J lines, the flux contributed by the CO gas at 1540 ± 80 K must be subtracted. In Figure 3*b*, we plot an expanded view of the low-J lines for AB Aur after subtracting the intensity contributed by the hot gas to each of the $J' = 0$–10 transitions. The extrapolation suggests that the fluxes of the $P(9)$–$P(11)$ lines are largely due to the hot gas and therefore are indicated as upper limits. In this case, the discontinuity near the $P(5)$ line [$J' = 4$ or $J'(J' + 1) = 20$] seen in Figure 3*b* results from optically thick gas. The opacity can be determined by considering the ratio of the flux of the $R(0)$ line to the $P(2)$ line. The Hönl-London formulae for $\Delta\Lambda = 0$ shows $S_J^R = J'$ and $S_J^P = J' + 1$. The intensity of an emission line is directly proportional to S_J (Herzberg 1950), so the flux of the $P(2)$ line should be twice that of the $R(0)$ line. The measured ratio of these lines is 1.1 ± 0.2 and can be explained by considering the effect of opacity on the observed gas. Using Beer's law, $I = I_0 e^{-\tau}$, the opacity of each line can be calculated. The opacity is given by $\tau = N_0 \sigma P_J$, where N_0 is the column density of CO in the $v'' = 0$ state, σ is the cross section of the transition, and P_J is the fractional population of molecules in the lower rotational state. Calculation of σ and P_J allows the determination of the column density and opacity for each observed line. The $P(5)$ line is maximally suppressed with a $\tau_5 = 2.3$.

Correcting the low-J lines for the calculated opacity, seen as a solid line in Figure 3*b*, provides a rotational temperature of 70 ± 10 K, which results from infrared fluorescence at the surface of the flared disk ($8 < R < 50$ AU).

For the hot CO, we can make an estimate of the column density. The column density of the gas is given by

$$N = \frac{4\pi F_{\rm line}}{\Omega g_{\rm line} hc\tilde{\nu}} \ ,$$

where $g_{\rm line}$ is the fluorescence efficiency for a given rovibrational transition by IR pumping (DiSanti et al. 2001). The fluorescence efficiency at 1 AU from the Sun for the $v = 1$–0 band (g_{0-1}) is 2.6×10^{-4} photons molecule^{-1} s^{-1}, and it is directly proportional to the flux of the IR radiation (Crovisier & Le Bourlot 1983; Weaver & Mumma 1984), and $g_{\rm line} = P_J g_{0-1}$. Using the ratio of the infrared luminosity of AB Aur to the Sun, the resulting g_{0-1} for AB Aur is 0.39 photons molecule^{-1} s^{-1} at a distance of 1 AU assuming no extinction. Dullemond et al. (2001) predicts that the inner rim of the disk of AB Aur is at 0.52 AU and at a temperature of 1500 K. Based on the calculated rotational temperature and excitation state of the gas, we suggest that the hot gas is located just inside the inner rim, where it is effectively shielded from UV radiation. If we assume that the CO is located at 0.6 AU, then $g_{0-1} = 1.1$ photons molecule^{-1} s^{-1}, and the column density of the observed CO is 2×10^{13} cm^{-2}. This represents a lower limit to the CO mass in AB Aur of 1×10^{21} g. The resolution element for our AB Aur observations is $0\farcs43 \times 0\farcs54$ and the distance to AB Aur is 144 pc; thus, our beam size is 5300 AU^2. Further modeling will be needed to better constrain the actual size of the hot CO emitting region. For the cold, optically thick CO, we are seeing only a small fraction of the gas, so it is not reasonable to estimate the column density and mass.

The observation and analysis of the CO spectra for AB Aur provide two important constraints for the structure of the disk. First, the hot CO component must be largely shielded from the rather strong UV radiation from the star, as the $v = 2$–1 and 3–2 transitions of CO are not detected. The implication is that the dust will quickly scatter UV, severely quenching UV excitation of the $v' = 2$ and 3 levels. The longer wavelength radiation can penetrate farther into the central inner disk region to a sufficient depth where a significant proportion of the $v = 1$–0 transitions of CO are excited to a high rotational temperature. Similarly, the UV must be effectively scattered from the outer disk regions, as the cold CO gas shows only fluorescence from infrared excitation. Second, the two-component temperature structure implies that we are observing two distinct regions of the disk.

The rotational temperatures of the CO can be used to place constraints on the approximate location of the gas from the central star. The model by Dullemond et al. (2001) for AB Aur indicates that the dust temperature ranges from 1500 to 400 K in the inner 1 AU and 400 to 150 K from 8 to 100 AU. It is just outward of the "puffed-up" rim, where the dust density is high, that we suggest the observed CO at 1500 K originates. The colder gas at 70 K must be located outside 8 AU, where the stellar radiation intercepts the flared disk beyond the shadowed region. For the outer disk the results suggest that the dust has scattered a large fraction of the UV, but sufficient IR radiation survives to excite the CO gas. Natta et al. (2001) noted that the flared disk likely intercepts less than 30% of the stellar UV and IR radiation. Figure 4 illustrates a possible scenario (see Dullemond et al. 2001) for AB Aur in which the hot CO is emitted from the dusty inner disk rim and the cold CO originates from the outer flared region of the disk.

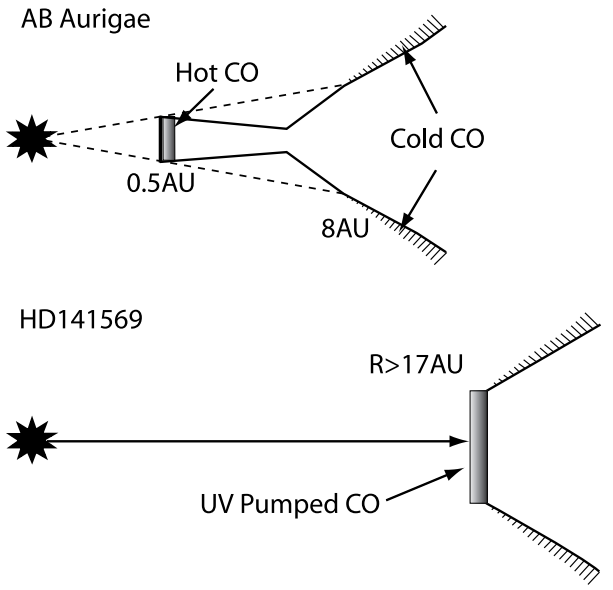

FIG. 4.—Flared disk diagrams for AB Aur and HD 141569. The top figure illustrates that the hot CO originates just beyond the rim of the inner disk and the cold CO originates from the flared disk at distances outward of 8 AU. The shadowed disk out to 8 AU does not contribute significantly to CO emission. The puffed-up dust in the inner disk (see Dullemond et al. 2001) scatters the UV radiation such that both the hot and cold CO result from infrared fluorescence (resonant scattering). The illustration for HD 141569 shows the inner disk region is cleared to a distance of approximately 17 AU where the CO is excited by UV radiation.

Similar temperature distributions from CO absorption lines have been observed from embedded young stellar objects where the two components include a contribution from warmer gas close to the star and colder gas in an extended foreground disk (Mitchell et al. 1990; Boogert, Hogerheijde, & Blake 2002). Our results indicate that the two components originate from the disk within 50 AU of AB Aur, since all of the observed CO lines have identical Doppler shifts, the lines are produced by IR excitation, and the line profiles are similar.

The velocity width of the CO lines can further constrain the inclination of the disk. Models of young disks predict that bulk motions of dust and gas around the disk are within a few percent of Keplerian orbital velocities (Adachi et al.1976). If we assume that the warm CO gas is located at 0.5 AU at the inner edge of the disk and is in Keplerian orbit, the orbital velocity is 64 km s^{-1}. From the observations (Fig. 1*c*), the CO lines have a FWHM of 5 pixels (20 km s^{-1} or a maximum Doppler velocity of ± 10 km s^{-1}); thus, the inclination of the disk is constrained to less than 9°. This constraint is inconsistent with $i = 65°$ used by Dullemond et al. (2001). As they note, the necessity of a large inclination is due to the simplifying assumption of a purely vertical rim. A rounded inner rim surface will allow more of the rim radiation to be emitted in polar directions, but incorporating it into the model was beyond the scope of that work.

4. CO IN HD 141569

The CO lines detected from HD 141569 (IRTF 2001 August) are presented in Figure 2. The lines are redshifted 19 ± 2 km s^{-1} from the line of sight. Correcting for the Earth's motion, the heliocentric velocity of the CO surrounding HD 141569 is -8 ± 2 km s^{-1}. This measurement is consistent to 1 σ with that reported for HD 141569 elsewhere (Dunkin et al. 1997; Frisch 1987); similarly, the submillimeter measurements of CO found a heliocentric velocity of -8 km s^{-1} for the outer regions (Zuckerman et al. 1995).

Assuming that the CO is distributed uniformly around the star in the form of a disk, the average width of CO lines constrains the deprojected orbital velocity to 11 ± 3 km s^{-1}. Assuming Keplerian orbital velocities, the width of the lines limit the distance of the material from the star to more than 17 AU (Brittain & Rettig 2002).

As in the previous section, observations of CO can characterize the inner disk ($R < 50$ AU) by providing a measure of the rotational temperature and density. The rotational temperature of the $v' = 1$ band of CO in HD 141569 is 190 ± 30 K (see Fig. 3*c*). In contrast to AB Aur, the observed CO line strengths from the $v = 2$–1 and 3–2 transitions are quite strong at about half the intensity of the $v = 1$–0 transitions and indicate that the CO is pumped by strong stellar UV radiation from the B9.5e/A0 star, probably at the star/disk interface. Even at 17 AU, the intense short-wavelength stellar radiation impinging on the star/disk interface can rapidly ionize the molecular hydrogen as well as dissociate much of the CO (see Fig. 4). Slightly farther into the disk, the softer UV not quenched by the H_2 and scattered by dust excites the $v = 2$–1 and 3–2 levels of CO. Using the $v = 1$–0, 2–1, and 3–2 vibrational bands, the column density of the detected CO gas is 10^{10}–10^{11} cm^{-2}. It is important to note that the resulting column density and CO mass (approximately 10^{19} g; Brittain & Rettig 2002) only represent material near the star/disk interface; thus only a fraction of the mass is detected. Any dust beyond this point quickly scatters the UV radiation, shielding the remainder of the CO.

There is no evidence that the CO emission is extended spatially beyond the PSF of the star ($\sim$50 AU), the region of planet formation of interest to this work. Beyond this distance, where most of the cold CO molecules are in the ground vibrational state, the near-IR observations are not sensitive. Submillimeter measurements of CO can measure the outer regions $<$130 AU, as noted by Zuckerman et al. (1995), who estimate 20–460 Earth masses of H_2 gas and approximately 10^{25} g of CO (or $\sim 10^{-3}$ Earth masses).

The CO results for HD 141569 show that not all the gas has been removed from the inner disk. However, the lack of gas at $R < 17$ AU shows that if the system has not already formed a planet or protoplanet, it is unlikely to contain sufficient quantities of gas to do so at this stage of disk clearing. The minimal content of CO in the inner disk compared to AB Aur confirms that the disk of HD 141569 is at a more advanced disk age and constrains the planet formation timescale as less than the age of HD 141569.

5. SUMMARY AND CONCLUSIONS

The detection of CO emission is important to quantify the evolution in preplanetary disk regions of HAeBe stars by constraining the gas dissipation rate and potential for planetary formation. For AB Aur, CO emission constrains the gas to two distinct locations (temperatures) within the inner 50 AU. The spectra indicate the CO excitation mechanism is predominantly via infrared radiation, as only the $v = 1$–0 lines are detected. The hotter component of the CO gas, having an effective rotational temperature of 1540 ± 80 K, likely results from gas in a "puffed-up" optically thin rim at distances slightly beyond the cleared inner gap region of $\sim$0.5 AU where the UV is strongly attenuated. The colder CO gas at 70 ± 10 K can be related to material in the outer flared disk region at distances beyond 8 AU, where it is effectively shielded from a large fraction of the stellar radiation (Natta et al. 2000; Dullemond et al. 2001). Additional high-resolution observations and modeling will constrain the disk structure and gas opacities further.

The rotational temperature of the CO emission in the more evolved HD 141569 is 190 ± 30 K and originates at or beyond the star/disk interface ($>$17 AU), where radiation clearing of the gas and dust and/or grain sublimation continues. Interestingly, the fraction of CO observed is excited by UV fluorescence. The lack of CO in the inner 17 AU rules out the possibility of active planet formation in this region and constrains the planet formation timescale to less than the age of HD 141569. It does not rule out the possibility that giant planet building has previously occurred and is helping to clear the inner regions of remaining gas and dust.

A long-standing question is whether protoplanetary cores can grow massive enough in the time available, before the gas is blown away, to permit the formation of gas giants around HAeBe stars. AB Aur has a massive young disk that extends inward very close to the central star, as evidenced by the infrared excess in the SED, and has sufficient gas to support the formation of gas giant planets. In contrast, HD 141569 shows a significantly reduced infrared excess in its SED (Malfait et al. 1998) and only a residual amount of CO in the inner disk. These differences suggest that the disk of AB Aur is comparatively young and active in contrast to the advanced evolutionary state of the disk around HD 141569. It is remarkable that the age difference between these two stars is only 1–3 Myr. This result implies that the gas and dust evident in AB Aur must be dissipated very quickly if it is an evolutionary precursor to HD 141569. Further modeling and observations of AB Aur and HD 141569 as well as other HAeBe stars will better constrain the dynamics of preplanetary disk evolution around young stars and provide further constraints on the current models of disk structure and the planet formation timescales.

We would like to thank the anonymous reviewer for many constructive comments. We would also like to thank J. Hahn for originally suggesting that we look at HD 141569. T. W. R. and S. D. B. were supported for this work under NSF Astronomy grant 02-05881.

REFERENCES

Adachi, I., Hayashi, C., & Nakazawa, K. 1976, Prog. Theor. Phys., 56, 1756
Backman, D. E., & Paresce, F. 1993, in Protostars and Planets III, ed. E. Levy & J. Lunine (Tucson: Univ. Arizona Press), 1253
Boogert, A. C. A., Hogerheijde, M. R., & Blake, G. A. 2002, ApJ, 568, 761
Bouwman, J., de Koter, A., van den Ancker, M. E., &Waters, L. B. F. M. 2000, A&A, 360, 213

Brittain, S. D., & Rettig, T. W. 2002, Nature, 418, 57
Carr, J. S., Mathieu, R. D., & Najita, J. R. 2001, ApJ, 551, 454
Catala, C., Czarny, J., Felenbok, P., & Praderie, F. 1986, A&A, 154, 103
Chiang, E. I., & Goldreich, P. 1999, ApJ, 519, 279
Chiang, E. I., Joung, M. K., Creech-Eakman, M. J., Qi, C., Kessler, J. E., Blake, G. A., & van Dishoeck, E. F. 2001, ApJ, 547, 1077
Crovisier, J., & Le Bourlot, J. 1983, A&A, 123, 61
DiSanti, M., Mumma, M., Dello Russo, N., & Magee-Sauer, K. 2001, Icarus, 153, 361
Dullemond, C. P., Dominik, C., & Natta, A. 2001, ApJ, 560, 957
Dunkin, S. D. Barlow, M. J., & Ryan, S. G. 1997, MNRAS, 286, 604
Finkenzeller, U., & Mundt, R. 1984, A&AS, 55, 109
Fisher, R., Telesco, C., Piña, R., Knacke, R., & Wyatt, M. 2000, ApJ, 532, L141
Frisch, P. C. 1987, ApJS, 65, 313
Gonzalez-Alfonso, E., Wright, C. M., Cernicharo, J., Rosenthal, D., Boonman, A. M. S., & van Dishoeck, E. F. 2002, A&A, 386, 1074
Grady, C. A., Woodgate, G., Bruhweiler, F. C., Boggess, A., Plait, P., Lindler, D. J., Clampin, M., & Kalas, P. 1999, ApJ, 523, L151
Herbig, G. H. 1960, ApJS, 4, 337
Herzberg, G. 1950, Spectra of Diatomic Molecules (New York: Van Nostrand Reinhold), 121
Hillenbrand, L., Strom, S., Vrba, F., & Keene, J. 1992, ApJ, 397, 613
Kunde, V. G., & Maguire W. C. 1974, J. Quant. Spectrosc. Radiat. Transfer, 14, 803
Malfait, K., Bogaert, E., & Waelkens, C. 1998, A&A, 331, 211
Mannings, V., & Sargent, A. 1997, ApJ, 490, 792
Marsh, Kenneth A., Van Cleve, J. E., Mahoney, M. J., Hayward, T. L., & Houck, J. R. 1995, ApJ, 451, 777
McLean, I. S., et al. 1998, Proc. SPIE, 3354, 566
Millan-Gabet, R., Schloerb, F. P., & Traub, W. A. 2001, ApJ, 546, 358
Millan-Gabet, R., Schloerb, F. P., Traub, W. A., Malbet, F., Berger, J. P., & Bregman, J. D. 1999, ApJ, 513, L131
Mitchell, G. F., Maillard, J. P., Allen, M., Beer, R., & Belcourt, K. 1990, ApJ, 363, 554
Mouillet, D., Lagrange, A. M., Augereau, J. C., & Ménard, F. 2001, A&A, 372, L61
Mumma, M. J., Stone, E. J., & Zipf, E. C. 1971, J. Chem. Phys., 54, 2627
Najita, J. R., Carr, J. S., Glassgold, A. E., Shu, F. H., & Tokunaga, A. T. 1996, ApJ, 462, 919
Najita, J. R., Edwards, S., Basri, G., & Carr, J. 2000, in Protostars and Planets IV, ed. V. Mannings, A. P. Boss, & S. S. Russell (Tucson: Univ. Arizona Press), 457
Nakajima, T., & Golimowski, D. A. 1995, ApJ, 444, L101
Natta, A., Grinin, V., & Mannings, V. 2000, in Protostars and Planets IV, ed. V. Mannings, A. P. Boss, & S. S. Russell (Tucson: Univ. Arizona Press), 559
Natta, A., Prusti, T., Neri, R., Wooden, D., Grinin, V. P., & Mannings, V. 2001, A&A, 371, 186
Prinn, R. G. 1993, in Protostars and Planets III, ed. E. Levy & J. Lunine (Tucson: Univ. Arizona Press), 1005
Roberge, A., et al. 2001, ApJ, 551, L97
Rothman, L. S., et al. 1992, J. Quant. Spectrosc. Radiat. Transfer, 48, 469
Sylvester, R. J., Skinner, C. J., Barlow, M. J., & Mannings, V. 1996, MNRAS, 279, 915
The, P. S., de Winter, D., & Perez, M. R. 1994, A&AS, 104, 315
Thi, W. F., et al. 2001, ApJ, 561, 1074
Tokunaga, A. T., Toomey, D., & Carr, J. 1990, in Instrumentation in Astronomy VII (Bellingham: Society of Photo-Optical Instrumentation Engineers), 131
van den Ancker, M. E. 1999, Ph.D. thesis, Univ. Amsterdam
van den Ancker, M. E., de Winter, D., & Tjin A Djie, H. R. 1998, A&A, 330, 145
van der Tak, F. F. S., van Dishoeck, E. F., Evans, N. J., II, & Blake, G. A. 2000, ApJ, 537, 283
Waters, L. B. F., & Waelkens, C. 1998, ARA&A, 36, 233
Weaver, H. A., & Mumma, M. J. 1984, ApJ, 276, 782
Weinberger, A. J., Rich, R., Becklin, E., Zuckerman, B., & Matthews, K. 2000, ApJ, 544, 937
Weinberger, A. J., et al. 1999, ApJ, 525, L53
Zuckerman, B., & Becklin, E. 1993, ApJ, 414, 793
Zuckerman, B., Forveille, T., & Kastner, J. H. 1995, Nature, 373, 494